Pressure-induced structural crossover in a $Zr_{65}Ni_{35}$ metallic glass

Dazhe Xu,[1] Hongbo Lou,[1,2] Di Peng,[2] Zhenfang Xing,[1,3] Fujun Lan,[1] Ziliang Yin,[1] Fei Zhang,[4] Lianghua Xiong,[5]
Zhidan Zeng,[1,2] Hongwei Sheng,[6,*] and Qiaoshi Zeng[1,2,†]

[1] *Center for High Pressure Science and Technology Advanced Research, Shanghai 201203, China*
[2] *Shanghai Key Laboratory of Material Frontiers Research in Extreme Environments (MFree),*
Institute for Shanghai Advanced Research in Physical Sciences (SHARPS), Shanghai 201203, China
[3] *State Key Laboratory of Superhard Materials, Institute of Physics, Jilin University, Changchun 130012, China*
[4] *Multi-Discipline Research Center, Institute of High Energy Physics, Chinese Academy of Sciences, Beijing 100049, China*
[5] *Shanghai Key Laboratory of Advanced High-Temperature Materials and Precision Forming, School of Materials Science*
and Engineering, Shanghai Jiao Tong University, Shanghai 200240, China
[6] *Department of Physics and Astronomy, George Mason University, Fairfax, Virginia 22030, USA*

(Received 21 February 2024; accepted 2 May 2024; published 13 May 2024)

The local atomic structure has long been recognized as a predominant characteristic and key to understanding glassy structures and properties. However, the factors governing the formation and evolution of these structures in metallic glasses remain elusive. Herein, we report an unexpected local structural crossover under pressure in a simple binary $Zr_{65}Ni_{35}$ metallic glass consisting of pure transition metals, evidenced by *in situ* high-pressure synchrotron x-ray diffraction and electrical resistivity measurements combined with *ab initio* molecular dynamics simulations. While the specific volume of the metallic glass (MG) follows a single-phase compression behavior without an apparent volume collapse, detailed analysis of the structural properties using structure factor, reduced pair-distribution function, and simulations reveals sharp changes of the Ni-centered clusters at ∼20 GPa in terms of their coordination numbers, atomic pair distances, and Voronoi polyhedra. This structural crossover is found to be closely linked to the enhanced contribution of the Ni *d* orbital to the electron density of state at the Fermi level under high pressures. These results underscore the correlation between the local atomic structure and the intricate electronic structure, particularly the 3*d* electronic structure, in transition-metal MGs, which sheds light on the stability characteristics of local structures in MGs from an electronic structure point of view.

DOI: 10.1103/PhysRevB.109.174111

I. INTRODUCTION

Comprehending the disordered atomic structure of glasses has remained a persistent challenge, impeding the targeted design and development of glasses at the atomic scale. Metallic glasses (MGs), with densely packed atomic structures resulting primarily from nondirectional metallic bonds, provide ideal “simple” model systems to address various glass problems [1–3]. Despite the lack of well-defined structural models for describing glass structures, it is widely accepted that local structures such as topological and chemical short-range order, along with medium-range order (MRO), play pivotal roles in understanding MGs [4–9].

External stimuli are recognized as potent tools for instigating structural modulation of disordered materials, presenting a powerful pathway for deeper exploration of their structural intricacies. Pressure, as a fundamental thermodynamic variable, has proven to be an effective and clean means of modulating the structures and properties of materials [10]. As applied pressure increases, the sample volume decreases, resulting in reduced interatomic distances and even significant modification of the electronic structure and chemical bonding. For most disordered materials, compression typically results in a more densely packed structure, often related to the variation in the packing scheme [11–13].

In the case of MGs, the typical densification effect induced by pressure is often negligible due to their inherently densely packed atomic structures under ambient conditions [4,14]. Recently, there has been a growing recognition that chemical interaction between different elements, or their electronic structures, could play a critical role in determining the atomic structures and properties of MGs, which could be highly tunable under high pressure. For instance, pressure-induced structural changes, such as polyamorphism in MGs, primarily arise from changes in the electronic structures [15–21]. Therefore, it is not surprising that in previous high-pressure experiments, pressure-induced polyamorphism or electronic structural changes has never been observed in the MGs systems comprising only regular transition metals with similar pressure-stable electronic structures, such as the prototype Zr-Cu MGs [22–24]. X-ray-diffraction (XRD) patterns taken on many MGs under high pressure typically retain a similar profile to that at ambient pressure, i.e., shifting elastically during compression [25]. Although the atomic structures of Zr-Cu and Zr-Ni binary MGs are similar, the distinctions in their electronic structures result in some discernible

---

[*] hsheng@gmu.edu

[†] zengqs@hpstar.ac.cn

©2024 American Physical Society

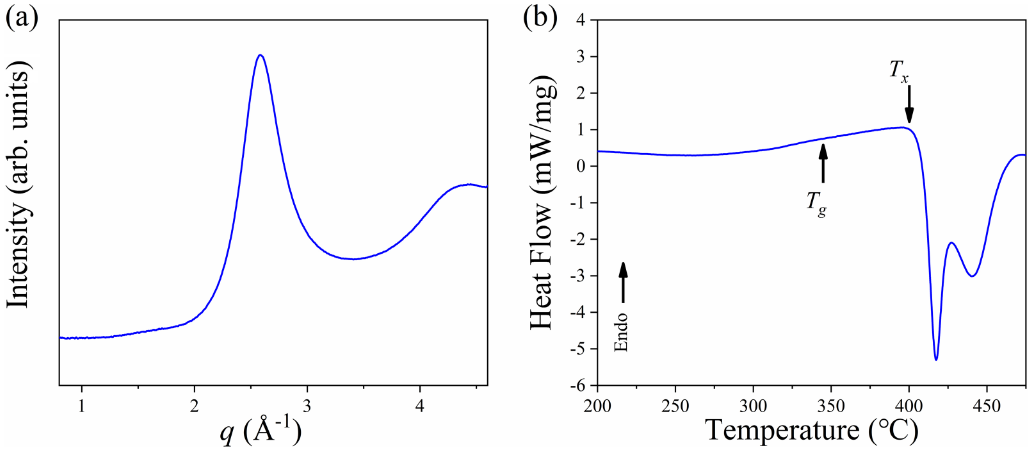

FIG. 1. Characterization of glassy features of the $Zr_{65}Ni_{35}$ MG sample at ambient pressure. (a) Synchrotron XRD revealing a typical amorphous peak. (b) DSC trace determining the glass transition (T_g) and crystallization (T_x) temperatures.

differences in properties [26–28]. Therefore, Zr-Cu and Zr-Ni MGs serve as ideal model systems to address the effect of electronic structure on MG structures, particularly with gradual modification and potentially amplified distinctions by high-pressure compression [29,30].

In this paper, we report a pressure-induced local structural crossover in a binary $Zr_{65}Ni_{35}$ MG. Through *in situ* high-pressure synchrotron XRD, we monitor the atomic structure evolution of the $Zr_{65}Ni_{35}$ MG up to 40 GPa. Consistent findings from the structure factor, $S(q)$, and the reduced pair-distribution function, $G(r)$, confirm the occurrence of local structural crossover during compression at approximately 20 GPa, but without any noticeable volume collapses or deviations from the initial trend. Analysis of the nearest-neighbor coordinate number (CN) and Voronoi polyhedral (VP) indices highlights that the structural crossover mainly involves the reconfiguration of Ni-centered clusters. Furthermore, *in situ* high-pressure electrical resistivity experiments reveal corresponding changes at the same critical pressure. These intriguing changes coincide with the modification of the Ni 3d orbital near ∼20 GPa, as elucidated by electronic structure calculations.

II. EXPERIMENTAL METHODS

A binary $Zr_{65}Ni_{35}$ (at. %) master ingot was prepared by arc melting of high-purity (>99.9 at. %) Zr and Ni raw materials. A high-purity argon atmosphere with a Ti ingot as an oxygen getter was used to prevent oxidation. The alloy ingot was flipped and remelted at least four times to ensure chemical homogeneity and then was quenched into amorphous ribbons with a thickness of ∼25 μm by single-roller melt spinning under a high-purity argon atmosphere. The amorphous nature was verified by synchrotron XRD experiment at the beamline 15U1 of Shanghai Synchrotron Radiation Faculty (SSRF) and a differential scanning calorimeter (DSC) (Perkin Elmer DSC 8000), as shown in Fig. 1.

The *in situ* high-pressure XRD experiments on the $Zr_{65}Ni_{35}$ MG were carried out at the beamline 13-ID-D of Advanced Photon Source (APS), Argonne National Laboratory (ANL), USA, with an x-ray wavelength of 0.3344 Å and a focused beam (∼3.5 × 4 μm^2) by a Kirkpatrick-Baez mirror system. The XRD patterns were collected by a Dectris Pilatus CdTe 1-M pixel array detector, and LaB_6 was used as a standard for calibration. The detector center was positioned as far from the x-ray beam as feasible, approximately 78 mm away, in order to get larger q coverage. The $Zr_{65}Ni_{35}$ MG ribbon samples were cut into flakes with sizes of ∼40 × 40 × 20 μm^3. A symmetric diamond-anvil cell (DAC) with an anvil culet size of ∼400 μm was used as the *in situ* high-pressure apparatus. Tiny ruby balls and a gold foil flake were loaded beside the sample as pressure calibrants. T301 stainless steel was used as the gasket, and helium was loaded as the best hydrostatic pressure-transmitting medium (PTM) [31]. An optical image of the *in situ* high-pressure XRD sample is shown in the inset of Fig. 2(b). Throughout the experiment, background scattering patterns were consistently collected following sample signal acquisition at each pressure point. Two-dimensional XRD images were integrated into the one-dimensional $I(q)$ patterns using the software DIOPTAS [32]. $S(q)$ and $G(r)$ were derived from $I(q)$ using the PDFGETX3 software package [33].

The *in situ* high-pressure resistivity measurement was performed using a DAC made of Be-Cu alloy with a diamond-anvil culet size of ∼300 μm. The gasket utilized in the experiments was made of rhenium. To insulate the circuit from the metallic rhenium gasket, a mixture of cubic BN and epoxy was employed as the insulator material. NaCl powder served as the PTM. The sample was cut into a dimension of ∼100 × 100 × 10 μm^3 and positioned at the center of the sample chamber above the NaCl PTM. A van der Pauw four-probe circuit employing platinum foil electrodes with a thickness of 4 μm was used for the resistivity measurement. A ruby ball was placed adjacent to the sample to calibrate the applied pressure. The electrical measurements were carried out using a Physical Property Measurement System (Quantum Design, USA). The alternating current was set to be 1 mA, and the temperature was maintained constantly at 300 K.

For theoretical calculations, in order to produce $Zr_{65}Ni_{35}$ MG from its melt, we performed *ab initio* molecular dynamics (MD) simulations using the density-functional

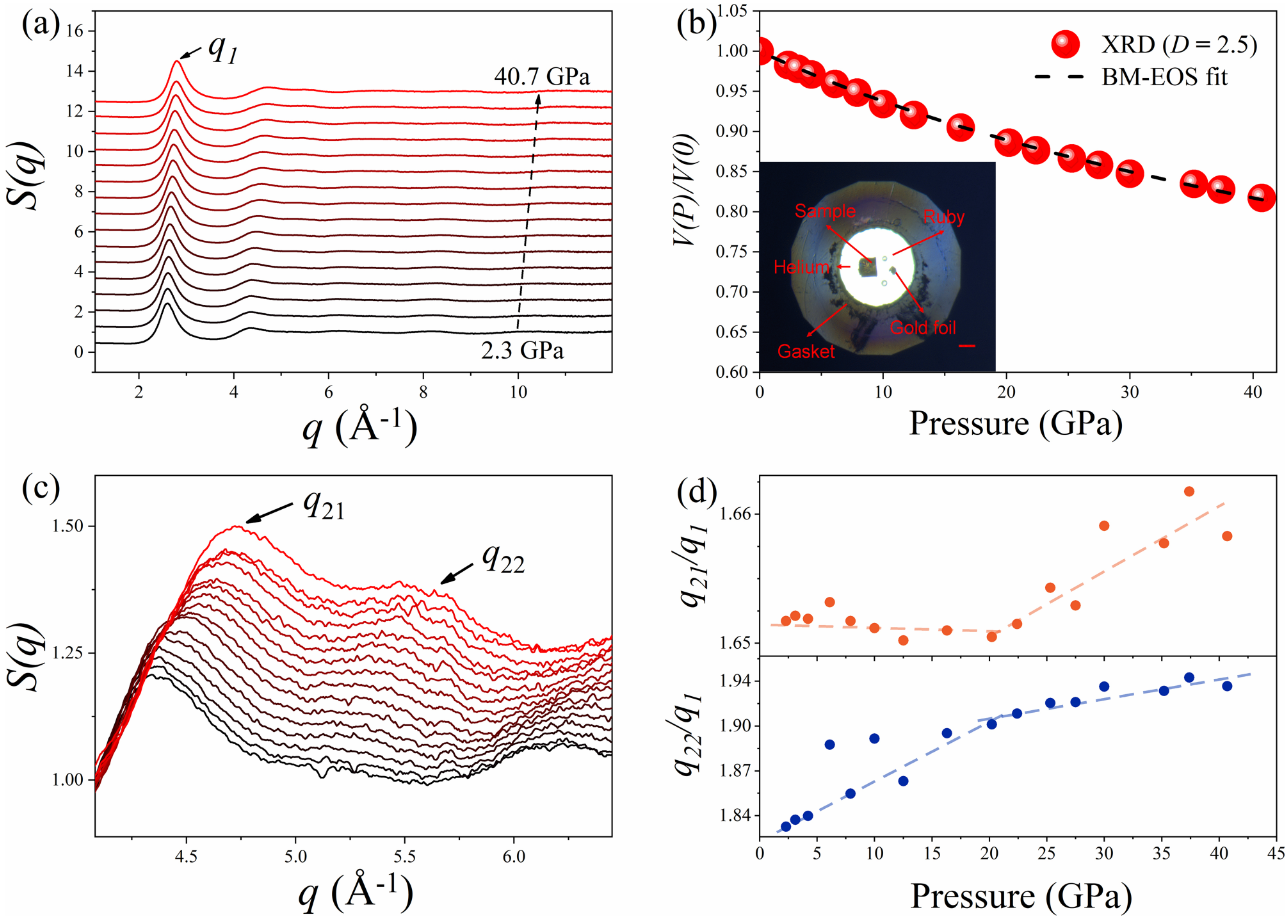

FIG. 2. Structure evolution of the $Zr_{65}Ni_{35}$ MG during compression from 2.3 to 40.7 GPa in reciprocal space. (a) Structure factor $S(q)$. (b) Relative volume change $V(P)/V(0)$ as a function of pressure obtained by the power law of the principal diffraction peak, $V(P)/V(0) = [q_1(0)/q_1(P)]^D$, where $D = 2.5$. The data point at 0 GPa was obtained outside DAC. The black dashed line is the fit to the third-order BM-EOS. Inset is the optical image of the sample loaded in a symmetric DAC for the *in situ* high-pressure XRD experiment. The scale bar represents 40 μm. (c) An enlarged plot of the evolution of the second peak of $S(q)$ during compression. (d) The peak position ratios of q_{21}/q_1 and q_{22}/q_1 as a function of pressure. The dashed lines are a guide to the eye, helping to easily identify the kink at ~20 GPa.

theory (DFT) as implemented in the Vienna *Ab initio* Simulation Package (VASP) [34]. Our simulations utilized the projector augmented-wave potential [35] and the generalized gradient approximation with valence configurations set at $3d^8\,4s^2$ for Ni and $4d^2\,5s^2$ for Zr. We set the kinetic energy cutoff at 400 eV and restricted our simulations to the gamma point. Our system, the liquid $Zr_{65}Ni_{35}$ comprising 250 atoms, was initially equilibrated at 0 GPa and 2000 K over a duration of 2 ps (1000 *ab initio* MD steps). Subsequently, it was quenched to 300 K at a rapid cooling rate of 1.25×10^{13} K/s within an *NPT* ensemble (maintaining a constant number of atoms, pressure, and enthalpy) with a time step of 2 fs. To simulate the processes of compression and decompression of the MG, we incrementally adjusted the size of the simulation box, achieved by a conjugate gradient geometric optimization to obtain the structure's minimum energy state at 0 K at different pressures.

III. RESULTS

Figure 2(a) shows the total structure factors, $S(q)$, of the binary $Zr_{65}Ni_{35}$ MG sample from 2.3 to 40.7 GPa. All $S(q)$ show smooth and broad patterns without any sharp Bragg peaks, indicating that the sample remains fully amorphous in the studied pressure range. With increasing pressure, all the $S(q)$ patterns shift to higher q values, which reflect the pressure-induced volume shrinkage or densification process as expected. Figure 2(b) displays the relative atomic volume change with increasing pressure, and the inset is the optical image of the sample loaded inside the DAC for *in situ* high-pressure XRD experiments. The relative atomic volume is calculated based on the relative change of the principal diffraction-peak position, q_1, in $S(q)$ by a power-law function, i.e., $V(P)/V(0) = [q_1(0)/q_1(P)]^D$, where $D = 2.5$ for Zr-based MGs under high pressure [36]. A total shrinkage in volume is estimated to be ~18% when the pressure is increased to 40.2 GPa. The evolution of the relative atomic volume $V(P)/V(0)$ can be well fitted to a third-order Birch-Murnaghan (BM) equation of state (BM-EOS) [37], with the isothermal bulk modulus $B_0 = 138.4 \pm 3.6$ GPa and the pressure derivative $B' = 3.6 \pm 0.2$ GPa, which are close to those of typical Zr-based MG [38]. The continuous *P-V* data, perfectly fitting a single BM-EOS, indicate the absence of a typical polyamorphic transition during compression. Besides

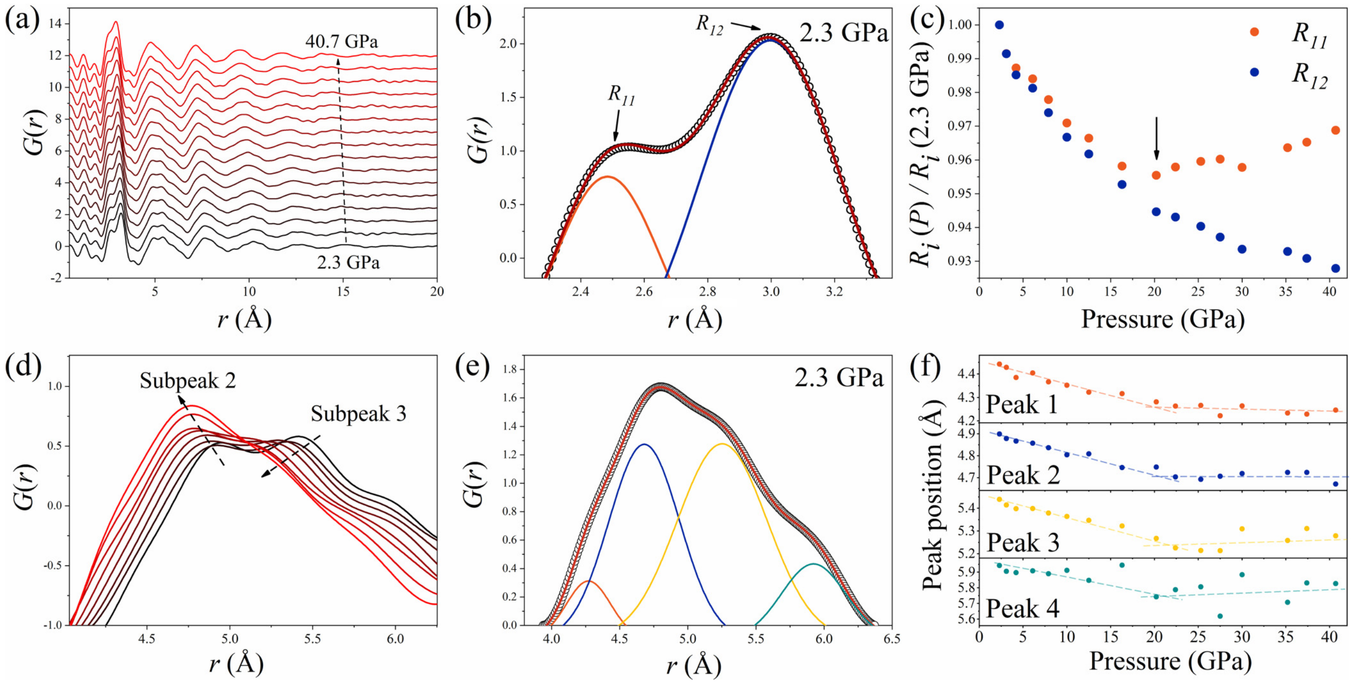

FIG. 3. Structure evolution of the $Zr_{65}Ni_{35}$ MG during compression from 2.3 to 40.7 GPa in real space. (a) The reduced pair-distribution functions, $G(r)$. (b) Representive deconvolution of the first peak of $G(r)$ into two Gaussian subpeaks, R_{11} and R_{12} (at 2.3 GPa). (c) The relative peak position of the two subpeaks as a function of pressure. (d) An enlarged plot of the evolution of the second peak of $G(r)$ during compression. (e) Representive deconvolution of the second peak of $G(r)$ into four Gaussian subpeaks (at 2.3 GPa). (f) The subpeak positions as a function of pressure. The dashed lines are a guide to the eye, helping to easily identify the kink at ∼20 GPa.

the first peak of $S(q)$, the second diffraction peak also carries rich information on local structures in atom packing. As shown in Fig. 2(c), the right shoulder of the second peak of $S(q)$ becomes increasingly apparent during compression. The main peak and the shoulder of the second peak are denoted as q_{21} and q_{22}, respectively. The peak position ratios of q_{21}/q_1 and q_{22}/q_1 shown in Fig. 2(d) can be used to estimate the deviation of local structures from ideal icosahedral packing [39,40]. Therefore, consistent kinks showing at ∼20 GPa in both ratios, q_{21}/q_1 and q_{22}/q_1 as a function of pressure, suggest a local structural crossover at ∼20 GPa.

To obtain more detailed insights into the structural crossover in the binary $Zr_{65}Ni_{35}$ MG in real space, the reduced pair-distribution function, $G(r)$, is derived from the Fourier transform of the $S(q)$ data. As shown in Fig. 3(a), at first glance, all atomic shells contract with increasing pressure. However, upon closer inspection, the first and second atomic shells undergo more intricate changes during compression, as indicated by the peak profile variation of the first and second peaks in $G(r)$. The first peak in $G(r)$ can be well fitted by two Gaussian subpeaks as shown in Fig. 3(b), e.g., R_{11} at ∼2.64 Å and R_{12} at ∼3.21 Å, respectively, at 2.3 GPa. According to the three atomic pairs with distinct distances ($R_{Zr-Zr} \approx 3.20$ Å, $R_{\mathrm{Zr-Ni}} \approx 2.84$ Å, and $R_{\mathrm{Ni-Ni}} \approx 2.48$ Å at 0 GPa) [41], it could be inferred that the first subpeak R_{11} mainly consists of the Zr-Ni and Ni-Ni atomic pairs while the second subpeak R_{12} mainly consists of the Zr-Zr atomic pair. Figure 3(c) shows the pressure dependence of normalized change of the two subpeak positions. Below ∼20 GPa, both peaks contract consistently with pressure. Interestingly, above ∼20 GPa, R_{12} decreases continuously following the initial low-pressure trend while R_{11} turns to increase with further compression. These results reveal a distinct signature of unusual structural crossover related to the Ni-Ni or Ni-Zr atomic pairs. Moreover, aside from the first peak, the second peak of $G(r)$ carries information on how atomic clusters (the first atomic shell) are connected to each other, forming extended structures, so-called MRO in MGs. As shown in Fig. 3(d), there are also dramatic changes in the peak profile of the second peak of $G(r)$. In a quantitative analysis based on the simplified hard-sphere model, the second peak of $G(r)$ typically can be fitted by four subpeaks, denoted as subpeaks-1,-2,-3, and -4, according to their peak positions from small to large, which represent four different connection schemes with different numbers of shared atoms from 4 to 1 between two adjacent clusters, denoted as 4-atom, 3-atom, 2-atom, and 1-atom connection methods, respectively [42,43]. The 4-subpeak fitting of the second peak of $G(r)$ is shown in Fig. 3(e). Consequently, the changes in peak profile with compression, as shown in Fig. 3(d), can be described by the relative variation in subpeak intensities, whereby the second subpeak intensity grows at the expense of the third subpeak intensity. In other words, the 2-atom shared connection is gradually replaced by the 3-atom shared connection scheme, suggesting a denser atomic packing during compression. In addition, regarding the subpeak positions as a function of pressure, as shown in Fig. 3(f), a consistent kink is observed at ∼20 GPa for all the four subpeaks, further confirming the presence of a structural crossover.

Furthermore, we conducted *ab initio* MD simulations to gain deeper insights into the structure. The reliability of the

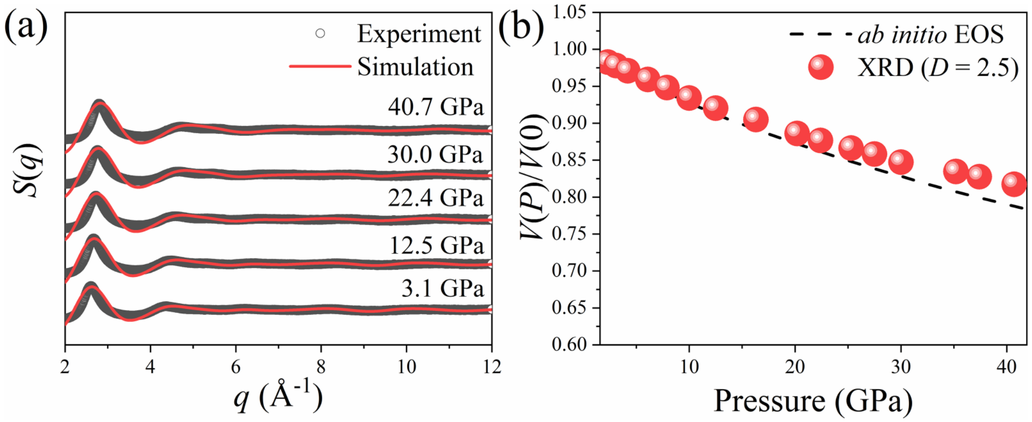

FIG. 4. Comparison of experimental and simulation results of the $Zr_{65}Ni_{35}$ MG. (a) Structure factors, $S(q)$. (b) Normalized sample volume $V(P)/V(0)$ vs pressure.

simulation results is verified by the satisfactory consistency in peak position and characteristics of $S(q)$ and the continuous pressure dependence of sample volume with those from experiments, as shown in Fig. 4. The compression behavior of three different atomic pairs during compression is elucidated by the simulations, as shown in Fig. 5(a). The total shrinkage of the Zr-Zr atomic pair is estimated to be ∼8.5% after compression to 40 GPa, while it is only ∼5.1 and ∼5.9% for the Zr-Ni and Ni-Ni atom pairs, respectively. The evolution of the nearest-neighbor averaged total coordinate number of Zr-centered and Ni-centered clusters with pressure is depicted in Fig. 5(b). While the average total CN of Zr atoms exhibits

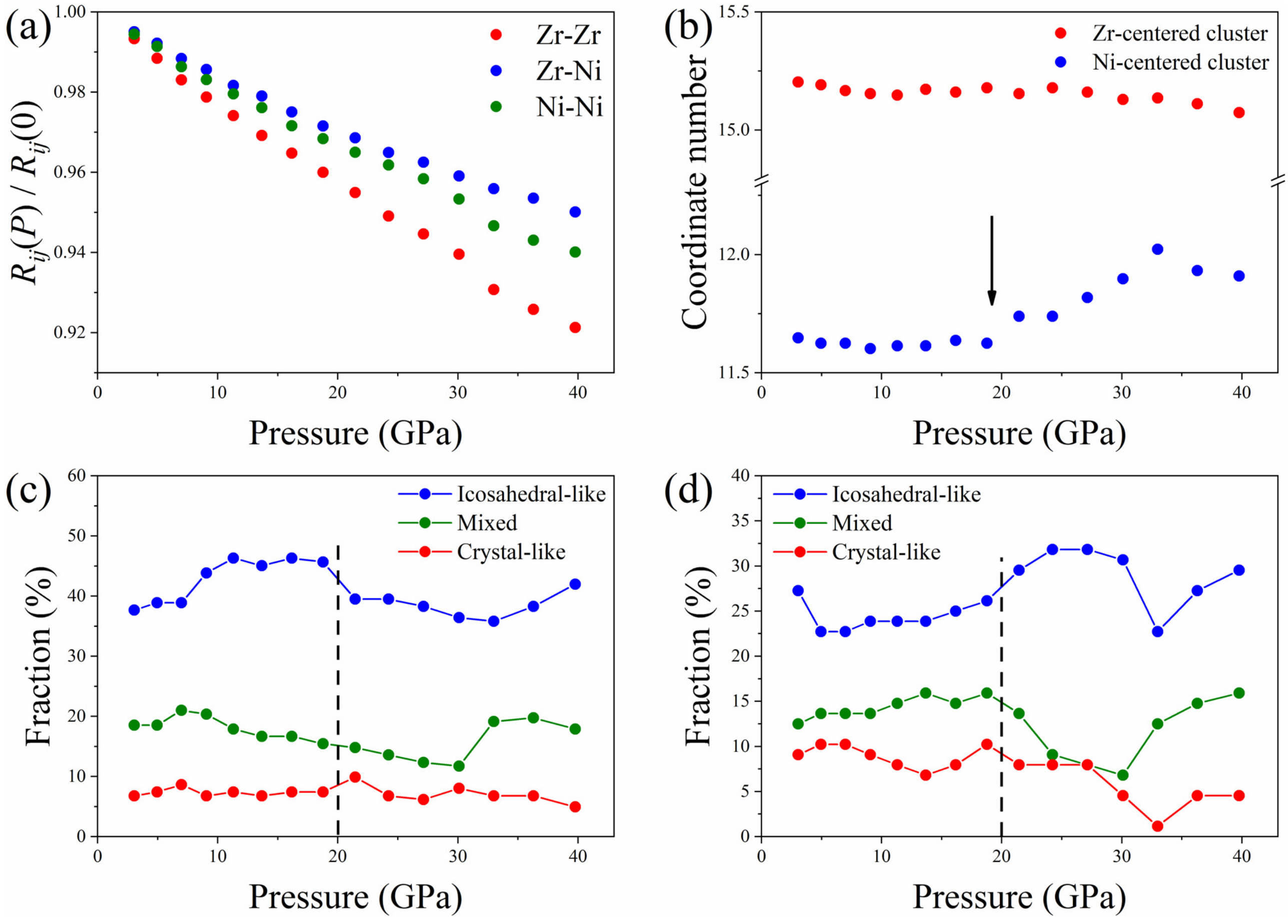

FIG. 5. Atomic structure evolution of the $Zr_{65}Ni_{35}$ MG during compression obtained by *ab initio* MD simulations. (a) Relative changes of the interatomic distances of the three atomic pairs. (b) The total CN of Zr- and Ni-centered clusters. The fraction evolution of different types of clusters with Zr (c) and Ni (d) as the center atoms.

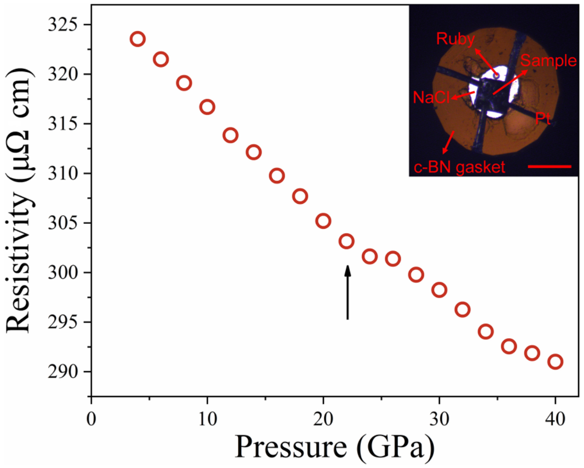

FIG. 6. *In situ* high-pressure electrical resistivity measurement on the $Zr_{65}Ni_{35}$ MG. A kink at ∼20 GPa is marked by the arrow. Inset is an optical image of the sample loaded in a symmetric DAC for the *in situ* high-pressure resistivity experiment. The scale bar represents 100 μm.

a slight decrease over the entire compression process, the averaged total CN of Ni atoms starts to increase with pressure above ∼20 GPa, suggesting that the structural crossover is more associated with Ni-centered clusters, with a noticeable increase in CN. As the total CN remains nearly constant at ∼14 during compression, the slight decrease in the CN of Zr atoms is compensated by the increase of the CN of Ni atoms. This aligns well with the experimental observation of opposite compression behaviors of the atomic pairs with compression above 20 GPa, as illustrated in Fig. 3(c). Based on the VP analysis of different clusters in the nearest-neighbor atomic shells, various clusters can be divided into three categories, i.e., icosahedral-like, crystal-like, and mixed clusters. VP configuration with indices such as $\langle 0, 0, 12, x\rangle$, $\langle 0, 1, 10, x\rangle$, and $\langle 0, 2, 8, x\rangle$ exhibiting fivefold symmetry with pentagonal faces are classified into icosahedral-like clusters (where x is typically between 0 and 4). VP configurations that possess more fourfold or sixfold symmetry with the indices of $\langle 0, 4, 4, x\rangle$ and $\langle 0, 5, 2, x\rangle$ are grouped into crystal-like clusters, while VPs with the index of $\langle 0, 3, 6, x\rangle$ are regarded as mixed clusters [44–46]. Figures 5(c) and 5(d) show the variation of the fraction of different VPs of Zr- and Ni-centered clusters, respectively. It is evident that icosahedral-like clusters predominantly populate the $Zr_{65}Ni_{35}$ MGs. In contrast to the minimal variation of Zr-centered clusters, the proportion of Ni-centered icosahedral-like clusters increases, and the crystal-like clusters decrease considerably above 20 GPa. Hence, structurally, the crossover can be more specifically attributed to the increase of icosahedral-like Ni-centered clusters during compression above ∼20 GPa.

Figure 6 illustrates the electrical resistivity measurement results of the $Zr_{65}Ni_{35}$ MG during compression up to ∼40 GPa. The electrical resistivity gradually decreases with increasing pressure, consistent with the typical compression behavior of MGs under high pressure [47]. In addition to the overall descending trend, a notable kink is observed at ∼22 GPa, indicating a resistivity signature of the structural crossover. It should be noted that the PTM used in the *in situ* high-pressure electrical resistivity experiment is solid NaCl, which is quasihydrostatic and could account for the slight pressure difference for the crossover observed in the resistivity and XRD experiments.

Considering the continuous change of sample volume (Fig. 2) alongside the discontinuity in resistivity, we hypothesize that the structural crossover may originate from electronic structural changes. To explore this further, we carried out electronic structure calculations for the sample below and above the structure crossover pressure using DFT calculations. Figure 7(a) displays the total density of states (DOS) and the projected density of states (PDOS) of electrons in the $Zr_{65}Ni_{35}$ MG at 3.1 and 43.2 GPa. As pressure increases, the distribution of the total DOS broadens and shifts to the lower-energy side. The broadened bandwidth of DOS indicates the delocalization of electrons induced by pressure. Moreover, it is evident that the d orbitals have a dominant contribution to the total DOS. Figure 7(b) provides a zoomed plot of the total DOS near the Fermi level at different pressures. The profile of DOS remains almost the same below 20 GPa but begins to vary between 21.5 and 24.2 GPa and gradually becomes distinct from those at low pressures. According to band theory, the DOS near the Fermi level determines the electronic conduction [48]. Figure 7(c) shows the evolution of DOS of d orbitals at the Fermi level during compression, in which a kink is seen between 20 and 30 GPa. According to the specific contribution fractions of the d orbitals of Zr and Ni to the total DOS, as shown in Fig. 7(d), the kink in Fig. 7(c) could be attributed to the sharp increase of contribution from Ni d orbital at almost the same pressure region with the structural crossover.

IV. DISCUSSION

The structural crossover in the $Zr_{65}Ni_{35}$ MG is unveiled by structural information derived from *in situ* high-pressure XRD data and electrical resistivity experiments, further validated by simulations, while the pressure dependence of the overall sample volume follows a single EOS without any collapse or anomalies. This could be interpreted as indicating that the local structural changes under high pressure resemble more of a cooperative structural rearrangement, preventing an overall density collapse. This finding underscores the complexity and adjustability of the local atomic structures of MGs under high pressure. The analysis of *in situ* high-pressure XRD combined with simulation results reveals considerable differences in compression behavior between different atomic pairs in the $Zr_{65}Ni_{35}$ MG. Diverse compressibility is commonly expected and observed in MG alloys. For instance, Zr-Cu binary MGs show hierarchic compression due to the much higher compressibility of Zr-Zr than the Zr-Cu and Cu-Cu atomic pairs [22,24]. However, there is no sign of structural polyamorphic transition or crossover observed in the Zr-Cu binary MGs during compression up to tens of GPa [22,24,41]. Therefore, it could be inferred that nonuniform compression among different atomic pairs does not necessarily result in structural transition or crossover in MGs. Recently, a local structural crossover without volume collapse during compression was reported in a senary high-entropy MG, which was ascribed to

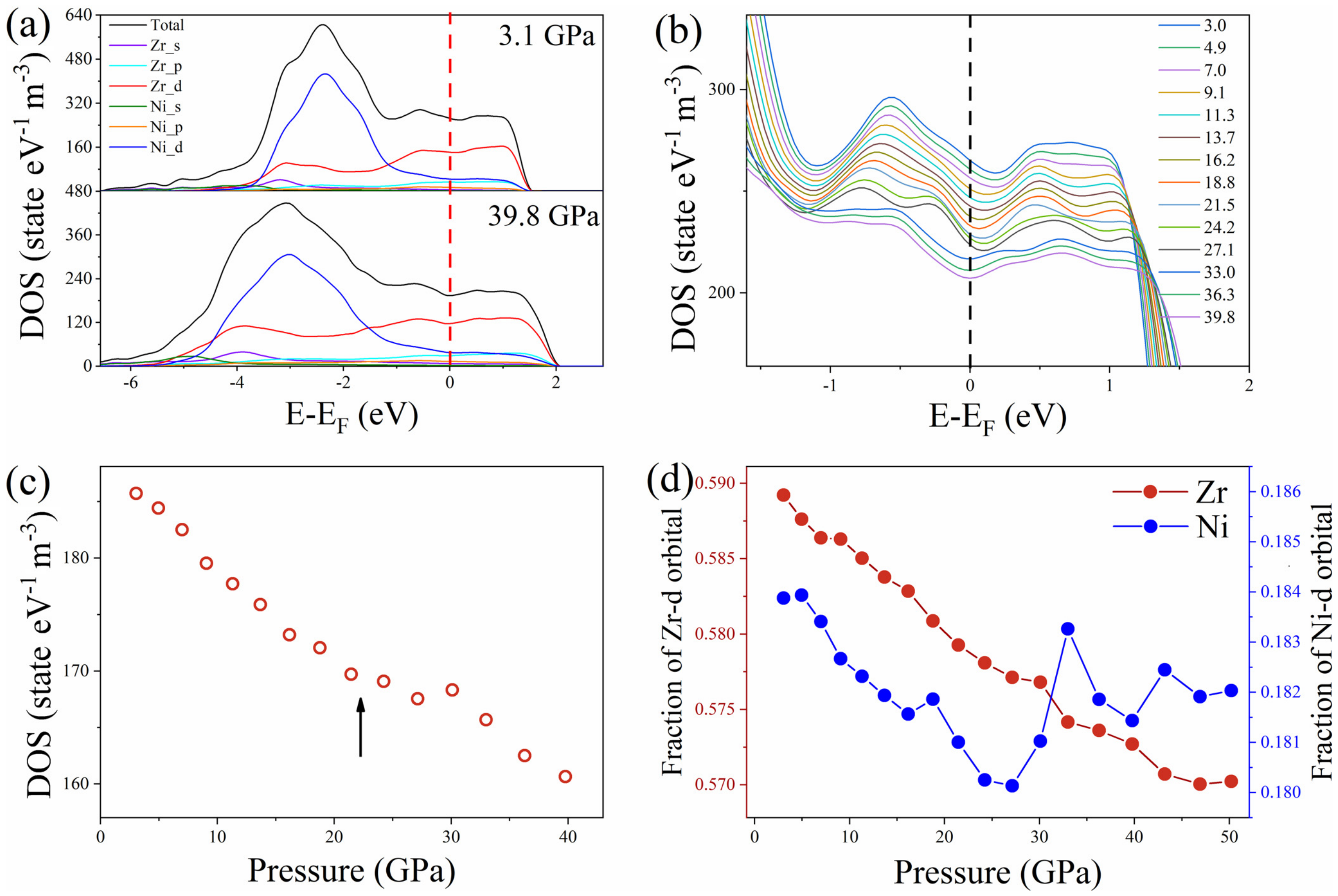

FIG. 7. The electronic structure evolution of the binary $Zr_{65}Ni_{35}$ MG during compression obtained by DFT calculations. (a) The electron DOS at 3.1 and 39.8 GPa. (b) A zoomed plot of the total DOS near the Fermi level during compression. (c) The pressure-dependent DOS of *d* orbitals at the Fermi level. A kink at ∼20 GPa is marked by the arrow. (d) The contribution of Zr and Ni *d* orbitals to the total DOS as a function of pressure.

the disproportional compression of various atomic pairs due to its extremely complex multicomponent nature [41]. In simple binary MGs, however, the effect of configurational entropy or complex chemical compositions is negligible.

Therefore, it is reasonable to speculate that the structural crossover may originate from the drastic modification of the electronic structure in the $Zr_{65}Ni_{35}$ MG during compression. Previous simulation and experiment results suggest that compared with the compositionally similar Zr-Cu MG systems, the directional bonding strength resulting from interactions between the *d* electrons is stronger in the Zr-Ni MG systems [28,49]. Therefore, despite the very close bonding distances between Zr–Cu (∼2.85 Å) and Zr–Ni (∼2.86 Å), Ni is likely to have a quite different effect from Cu on the electronic structures, leading to the distinct behaviors of these two MGs under high pressure. This scenario is supported by the quite unusual changes in the pressure-dependent Ni-centered clusters packing (Figs. 3 and 5) and *d*-electron contribution to the total DOS [Fig. 5(d)]. The electronic structural changes are expected to affect the interaction between atoms, and consequently alter the atomic packing arrangements [49].

Electronic resistivity is typically highly sensitive to both atomic and electronic structure variations. The pressure-dependent electronic resistivity of the $Zr_{65}Ni_{35}$ MG indeed shows a kink (Fig. 6) akin to the observation of the DOS of *d* electrons at the Fermi level [Fig. 7(c)]. Various theoretical models have been proposed to offer a quantitative description of the electrical resistivity of MGs. In the two-level tunneling model, the electrical resistivity decreases when the degree of structural disorder or free-volume content diminishes [50,51]. During compression, the free volume of MG is usually linearly compressed [52], leading to a monotonic linear decrease of resistivity as well without any discontinuity. Another widely accepted theory of electrical resistivity is the Ziman theory, first proposed in pure liquid metals [53], and its extended formula was later applied in MGs [54]. In our binary $Zr_{65}Ni_{35}$ MG, however, the Fermi level is located in the *d* band, so that the resonant scattering is too strong to be neglected [55]. According to the $s - d$ scattering model by Mott [56], the dominant contribution to the electrical resistivity comes from the scattering of *sp* electrons into empty *d* holes, which means that the resistivity is proportional to the DOS of the *d* orbitals at the Fermi energy. Our results, as shown in Figs. 6 and 7(c), align well with the Mott model, elucidating why the electrical resistivity decreases during compression with a kink at ∼20 GPa, coinciding with the pressure dependence of DOS of *d* orbitals.

The crossover in the structural configuration and resistivity of the $Zr_{65}Ni_{35}$ MG during compression is attributed to the same electronic mechanism, specifically related to the unusual behavior of Ni *d* orbital under high pressure. However, the overall volume change is continuous during compression. This characteristic sets it apart from the typical pressure-induced polyamorphic transitions reported before in MGs, which also have an electronic origin but are all accompanied by volume-change anomalies. For instance, pressure-induced volume collapse in the rare-earth element-based MGs due to delocalization of $4f$ electrons [17]; pressure-induced volume deviation from the initial low-pressure trend described by a single BM-EOS caused by the charge transfer between different elements in Ca-Al [18], Pd-Ni-P [19], and Pd-Ni-S [57] MGs. However, electronic structure calculations, as shown in Fig. 7(a), indicate no sharp electronic transition or charge transfer observed in the $Zr_{65}Ni_{35}$ MG during compression. Instead, as an MG consisting of pure transition metals, the *d* orbitals near the Fermi level play a dominant role; a kink in the contribution fraction of Ni *d* electrons to the total DOS at ∼20 GPa results in corresponding unusual changes in the electronic resistivity and the packing of Ni-centered clusters. It should be noted that this type of electronic structural modulation with Ni *d* electrons is relatively moderate compared with the charge transfer or electron delocalization reported in other polyamorphous MGs. As a result, the specific volume (density) change of the $Zr_{65}Ni_{35}$ MG sample remains continuous throughout compression.

V. CONCLUSIONS

In summary, we investigated the structural evolution of the binary $Zr_{65}Ni_{35}$ MG during compression using *in situ* high-pressure synchrotron XRD, electronic resistivity measurement, and *ab initio* MD simulations. While the overall volume (density) of the $Zr_{65}Ni_{35}$ MG sample decreases continuously, a local structural crossover is identified at ∼20 GPa. This crossover is characterized by considerable packing changes primarily associated with the Ni-centered clusters, accompanied by a kink in electrical resistivity at the same critical pressure. The underlying mechanism is attributed to pressure-induced electronic structural modulation of Ni *d* orbitals at ∼20 GPa, which is distinct from the traditional polyamorphism in MGs with sample volume anomalies. These findings suggest such structural crossover could be prevalent in other MGs and highlight the vital role of electronic structure on the structure and properties of MGs.

ACKNOWLEDGMENTS

The authors acknowledge financial support from Shanghai Key Laboratory of Material Frontiers Research in Extreme Environments, China (Grant No. 22dz2260800), the Shanghai Science and Technology Committee, China (Grant No. 22JC1410300), and the National Natural Science Foundation of China (Grant No. 52101187). *In situ* high-pressure XRD experiments were performed at beamline 13-ID-D, GSECARS (GeoSoilEnviroCARS), APS, ANL, USA. Synchrotron XRD experiments at ambient condition were carried out at the beamline 15U1 of Shanghai Synchrotron Radiation Faculty (SSRF), China. The authors are grateful to Dr. Vitali Prakapenka and Dr. Stella Chariton from GSECARS for their kind help with the synchrotron experiments, and Dr. Haiyun Shu from HPSTAR for his kind help with the gas loading. Use of the beamline 13- ID-D at GSECARS was supported by the National Science Foundation (NSF)-Earth Sciences (Grant No. EAR-1634415). APS is supported by the DOE Office of Science (Grant No. DE-AC02-06CH11357).

---

[1] W. H. Wang, C. Dong, and C. H. Shek, Bulk metallic glasses, Mater. Sci. Eng. R Rep. **44**, 45 (2004).
[2] Y. Q. Cheng and E. Ma, Atomic-level structure and structure–property relationship in metallic glasses, Prog. Mater. Sci. **56**, 379 (2011).
[3] M. Chen, A brief overview of bulk metallic glasses, NPG Asia Mater. **3**, 82 (2011).
[4] D. B. Miracle, A structural model for metallic glasses, Nat. Mater. **3**, 697 (2004).
[5] H. W. Sheng, W. K. Luo, F. M. Alamgir, J. M. Bai, and E. Ma, Atomic packing and short-to-medium-range order in metallic glasses, Nature (London) **439**, 419 (2006).
[6] D. Ma, A. D. Stoica, and X. L. Wang, Power-law scaling and fractal nature of medium-range order in metallic glasses, Nat. Mater. **8**, 30 (2009).
[7] Q. Zeng, H. Sheng, Y. Ding, L. Wang, W. Yang, J.-Z. Jiang, L. Mao Wendy, and H.-K. Mao, Long-range topological order in metallic glass, Science **332**, 1404 (2011).
[8] A. Hirata, P. Guan, T. Fujita, Y. Hirotsu, A. Inoue, A. R. Yavari, T. Sakurai, and M. Chen, Direct observation of local atomic order in a metallic glass, Nat. Mater. **10**, 28 (2011).
[9] Q. An, K. Samwer, M. D. Demetriou, M. C. Floyd, D. O. Duggins, W. L. Johnson, and W. A. Goddard, How the toughness in metallic glasses depends on topological and chemical heterogeneity, Proc. Natl. Acad. Sci. USA **113**, 7053 (2016).
[10] L. Zhang, Y. Wang, J. Lv, and Y. Ma, Materials discovery at high pressures, Nat. Rev. Mater. **2**, 17005 (2017).
[11] S. Sastry and C. Austen Angell, Liquid–liquid phase transition in supercooled silicon, Nat. Mater. **2**, 739 (2003).
[12] O. Mishima and H. E. Stanley, The relationship between liquid, supercooled and glassy water, Nature (London) **396**, 329 (1998).
[13] D. Wakabayashi, N. Funamori, and T. Sato, Enhanced plasticity of silica glass at high pressure, Phys. Rev. B **91**, 014106 (2015).
[14] Y. Yang, J. Zhou, F. Zhu, Y. Yuan, D. J. Chang, D. S. Kim, M. Pham, A. Rana, X. Tian, Y. Yao *et al.*, Determining the three-dimensional atomic structure of an amorphous solid, Nature (London) **592**, 60 (2021).
[15] H. W. Sheng, H. Z. Liu, Y. Q. Cheng, J. Wen, P. L. Lee, W. K. Luo, S. D. Shastri, and E. Ma, Polyamorphism in a metallic glass, Nat. Mater. **6**, 192 (2007).
[16] Q. S. Zeng, Y. C. Li, C. M. Feng, P. Liermann, M. Somayazulu, G. Y. Shen, H. K. Mao, R. Yang, J. Liu, T. D. Hu *et al.*, Anomalous compression behavior in lanthanum/cerium-based

metallic glass under high pressure, Proc. Natl. Acad. Sci. USA **104**, 13565 (2007).

[17] Q. S. Zeng, Y. Ding, W. L. Mao, W. Yang, S. V. Sinogeikin, J. Shu, H. K. Mao, and J. Z. Jiang, Origin of pressure-induced polyamorphism in $Ce_{75}Al_{25}$ metallic glass, Phys. Rev. Lett. **104**, 105702 (2010).

[18] M. Wu, H. Lou, J. S. Tse, H. Liu, Y. Pan, K. Takahama, T. Matsuoka, K. Shimizu, and J. Jiang, Pressure-induced polyamorphism in a main-group metallic glass, Phys. Rev. B **94**, 054201 (2016).

[19] Q. Du, X.-J. Liu, Q. Zeng, H. Fan, H. Wang, Y. Wu, S.-W. Chen, and Z.-P. Lu, Polyamorphic transition in a transition metal based metallic glass under high pressure, Phys. Rev. B **99**, 014208 (2019).

[20] G. Li, Y. Y. Wang, P. K. Liaw, Y. C. Li, and R. P. Liu, Electronic structure inheritance and pressure-induced polyamorphism in lanthanide-based metallic glasses, Phys. Rev. Lett. **109**, 125501 (2012).

[21] Q. Luo, G. Garbarino, B. Sun, D. Fan, Y. Zhang, Z. Wang, Y. Sun, J. Jiao, X. Li, P. Li *et al.*, Hierarchical densification and negative thermal expansion in Ce-based metallic glass under high pressure, Nat. Commun. **6**, 5703 (2015).

[22] J. Antonowicz, A. Pietnoczka, G. A. Evangelakis, O. Mathon, I. Kantor, S. Pascarelli, A. Kartouzian, T. Shinmei, and T. Irifune, Atomic-level mechanism of elastic deformation in the Zr-Cu metallic glass, Phys. Rev. B **93**, 144115 (2016).

[23] P. Dziegielewski, O. Mathon, I. Kantor, S. Pascarelli, T. Shinmei, T. Irifune, and J. Antonowicz, High pressure atomic structure of Zr–Cu metallic glass via EXAFS spectroscopy and molecular dynamics simulations, High Press. Res. **40**, 54 (2019).

[24] S. Luo, J. C. Khong, D. Daisenberger, S. Huang, P. F. McMillan, and J. Mi, Synchrotron x-ray total scattering and modeling study of high-pressure-induced inhomogeneous atom reconfiguration in an equiatomic $Zr_{50}Cu_{50}$ metallic glassy alloy, Phys. Rev. B **105**, 064203 (2022).

[25] N. Mattern, J. Bednarcik, H.-P. Liermann, and J. Eckert, Structural behaviour of $Pd_{40}Cu_{30}Ni_{10}P_{20}$ metallic glass under high pressure, Intermetallics **38**, 9 (2013).

[26] Z. Altounian and J. O. Strom-Olsen, Superconductivity and spin fluctuations in M-Zr metallic glasses ($M =$ Cu, Ni, Co, and Fe), Phys. Rev. B **27**, 4149 (1983).

[27] I. Bakonyi, Electronic properties and atomic structure of (Ti, Zr, Hf) (Ni, Cu) metallic glasses, J. Non-Cryst. Solids **180**, 131 (1995).

[28] A. Hirata, T. Morino, Y. Hirotsu, K. Itoh, and T. Fukunaga, Local atomic structure analysis of Zr-Ni and Zr-Cu metallic glasses using electron diffraction, Mater. Trans. JIM **48**, 1299 (2007).

[29] J. Destry, M. E. Amrani, and R. W. Cochrane, Pressure dependence of the room-temperature resistance of $Co_{100-x}Zr_x$ and $Fe_{100-x}Zr_x$ glasses, Phys. Rev. B **31**, 2499 (1985).

[30] Y.-z. Guo and M. Li, Atomistic simulation of a NiZr model metallic glass under hydrostatic pressure, Appl. Phys. Lett. **94**, 051901 (2009).

[31] X. Chen, H. Lou, Z. Zeng, B. Cheng, X. Zhang, Y. Liu, D. Xu, K. Yang, and Q. Zeng, Structural transitions of 4:1 methanol–ethanol mixture and silicone oil under high pressure, Matter Radiat. Extrem. **6**, 038402 (2021).

[32] C. Prescher and V. B. Prakapenka, DIOPTAS: A program for reduction of two-dimensional X-ray diffraction data and data exploration, High Press. Res. **35**, 223 (2015).

[33] P. Juhas, T. Davis, C. L. Farrow, and S. J. L. Billinge, *PDFgetX3:* A rapid and highly automatable program for processing powder diffraction data into total scattering pair distribution functions, J. Appl. Crystallogr. **46**, 560 (2013).

[34] G. Kresse and J. Hafner, Ab initio molecular dynamics for liquid metals, Phys. Rev. B **47**, 558 (1993).

[35] P. E. Blöchl, Projector augmented-wave method, Phys. Rev. B **50**, 17953 (1994).

[36] Q. S. Zeng, Y. Kono, Y. Lin, Z. D. Zeng, J. Y. Wang, S. V. Sinogeikin, C. Park, Y. Meng, W. G. Yang, H. K. Mao, and W. L. Mao, Universal fractional noncubic power law for density of metallic glasses, Phys. Rev. Lett. **112**, 185502 (2014).

[37] F. Birch, Finite elastic strain of cubic crystals, Phys. Rev. **71**, 809 (1947).

[38] W. H. Wang, The elastic properties, elastic models and elastic perspectives of metallic glasses, Prog. Mater. Sci. **57**, 487 (2012).

[39] H. W. Sheng, E. Ma, H. Z. Liu, and J. Wen, Pressure tunes atomic packing in metallic glass, Appl. Phys. Lett. **88**, 171906 (2006).

[40] T. Schenk, D. Holland-Moritz, V. Simonet, R. Bellissent, and D. M. Herlach, Icosahedral short-range order in deeply undercooled metallic melts, Phys. Rev. Lett. **89**, 075507 (2002).

[41] X. Zhang, H. Lou, F. Zhang, H. Luan, T. Liang, S. Li, X. Chen, Y. Shao, K.-F. Yao, Z. Zeng *et al.*, Pressure-induced local structural crossover in a high-entropy metallic glass, Phys. Rev. B **105**, 224201 (2022).

[42] S. P. Pan, J. Y. Qin, W. M. Wang, and T. K. Gu, Origin of splitting of the second peak in the pair-distribution function for metallic glasses, Phys. Rev. B **84**, 092201 (2011).

[43] J. Ding and E. Ma, Computational modeling sheds light on structural evolution in metallic glasses and supercooled liquids, npj Comput. Mater. **3**, 9 (2017).

[44] J. Finney, Random packings and the structure of simple liquids. I. The geometry of random close packing, Proc. R. Soc. London A **319**, 479 (1970).

[45] S. Trady, A. Hasnaoui, and M. Mazroui, Atomic packing and medium-range order in Ni_3Al metallic glass, J. Non-Cryst. Solids **468**, 27 (2017).

[46] Y. Zhang, H. Liu, J. Mo, M. Wang, Z. Chen, Y. He, W. Yang, and C. Tang, Atomic-level crystallization in selective laser melting fabricated Zr-based metallic glasses, Phys. Chem. Chem. Phys. **21**, 12406 (2019).

[47] T. Liang, F. Zhang, X. Zhang, X. Chen, S. Chen, H. Lou, Z. Zeng, D. Xu, K. Yang, Y. Xiao *et al.*, Pressure-induced spin crossover in a $Fe_{78}Si_9B_{13}$ metallic glass, J. Appl. Phys. **129**, 165901 (2021).

[48] S. R. Nagel, Thermoelectric power and resistivity in a metallic glass, Phys. Rev. Lett. **41**, 990 (1978).

[49] L. Huang, C. Z. Wang, S. G. Hao, M. J. Kramer, and K. M. Ho, Atomic size and chemical effects on the local order of Zr_2M ($M =$ Co, Ni, Cu, and Ag) binary liquids, Phys. Rev. B **81**, 014108 (2010).

[50] R. W. Cochrane, R. Harris, J. O. Ström-Olson, and M. J. Zuckermann, Structural manifestations in amorphous

alloys: Resistance minima, Phys. Rev. Lett. **35**, 676 (1975).

[51] M. Banville and R. Harris, Tunneling states in metallic glasses: A structural model, Phys. Rev. Lett. **44**, 1136 (1980).

[52] S. Chen, D. Xu, X. Zhang, X. Chen, Y. Liu, T. Liang, Z. Yin, S. Jiang, K. Yang, J. Zeng *et al.*, Reversible linear-compression behavior of free volume in a metallic glass, Phys. Rev. B **105**, 144201 (2022).

[53] J. M. Ziman, A theory of the electrical properties of liquid metals. I: The monovalent metals, Philos. Mag. **6**, 1013 (1961).

[54] P. J. Cote and L. V. Meisel, Resistivity in amorphous and disordered crystalline alloys, Phys. Rev. Lett. **39**, 102 (1977).

[55] E. Esposito, H. Ehrenreich, and C. D. Gelatt, Electrical transport in transition-metal liquids and metallic glasses, Phys. Rev. B **18**, 3913 (1978).

[56] N. F. Mott, The electrical resistivity of liquid transition metals, Philos. Mag. **26**, 1249 (1972).

[57] A. Fadhil, Y. Su, K. Glazyrin, D. Jiang, X. Wang, Q. Cao, D. Zhang, C. Gao, and J.-Z. Jiang, Pressure-induced atomic packing change in $Pd_{37}Ni_{37}S_{26}$ metallic glass, Acta Mater. **216**, 117116 (2021).